Proceedings of ASME Turbo Expo 2011
GT2011
June 6-10, 2011, Vancouver, British Columbia, Canada

GT2011-45126

COMBUSTOR AND AUGMENTOR COMBUSTION MODELING FOR LES BASED ON STOCHASTIC MODEL PARAMETERIZATION

William H. Calhoon, Jr. and Andrea C. Zambon
Combustion Research and Flow Technology, Inc. (CRAFT Tech)
Huntsville, AL and Pipersville, PA 18947, USA

and

Balu Sekar and Barry Kiel
Air Force Research Lab, AFRL/RZTC
Wright-Patterson Air Force Base, OH 45433, USA

ABSTRACT

A new modeling formulation for turbulent chemistry interactions in large eddy simulation (LES) is presented that is based on a unique application of the linear-eddy model (LEM) that includes large scale strain effects. This novel application of the LEM may be used to predict turbulent flame extinction limits due to both small and large scale strain effects. Statistics from this modeling formulation may be used to generate an inexpensive run-time model for LES predictions. This paper presents the LEM modeling formulation and demonstrates the capabilities of the approach for augmentor conditions. A methodology is also presented to formulate a LES subgrid model based on the simulation data.

INTRODUCTION

Advanced computational methodologies such as large-eddy simulation (LES) are required to evaluate design concepts for combustors and augmentors in high performance aircraft engines. However, LES is limited by the sub-models used to account for turbulence-chemistry interactions. For LES, turbulent combustion models span a wide spectrum of generality. On the low end of the spectrum are *moment methods* (e.g., eddy dissipation concept model [1], laminar flamelet model [2]) which employ a variety of simplifying assumptions to develop computationally affordable models that are relatively general. On the high end of the spectrum are stochastic methods (i.e., LES-LEM [3][4], pdf evolution equation method [5]) that seek to model the physics of the flow in a comprehensive fashion. These stochastic methods are accurate and general, but are very expensive computationally and become intractable for large chemical mechanisms.

There is a wide disparity between the modeling capabilities and computational cost of moment and stochastic methods. Moment methods sacrifice physics by *specifying* the shape the subgrid probability distribution function (pdf) of the reacting scalars in order to develop a computationally affordable model. On the other hand, stochastic methods retain the physics through a *prediction* of the subgrid pdf, but at a much greater computational cost. Currently there are very few models between moment methods that employ an assumed pdf approach and full stochastic methods that directly predict the pdf. With this in mind, the aim of this research is to develop a predictive methodology that is *between* current moment and stochastic methods with regard to computational cost and the ability to model the physics of the flow. This may be accomplished through a *parameterization* of the linear-eddy model (LEM) [6][7]. The LEM is a comprehensive mixing model that separately treats molecular diffusion (with finite-rate kinetics) and small scale turbulent stirring. Because the model resolves the microscale flame structure, extinction and re-ignition may be accurately captured.

Statistics from the LEM may be parameterized to form a computationally inexpensive run time model. Parameterization entails characterizing the model's statistics in terms of a reduced set of variables. In this approach, statistics required to close the filtered LES transport equations are derived from stand-alone LEM simulations that are parameterized in terms of

a set of characteristic variables. These statistics are stored in a database that may be deployed within a LES solver for a predictive calculation. The LES solver then recalls the required closure statistics from the database in a fast and efficient manner. Consequently, the parameterized LEM subgrid scale formulation is computationally *inexpensive* because the model statistics are *precomputed* and are not generated during the LES run. However, the model does include all the physics of the underlying stochastic model, including a *prediction* of the subgrid pdf.

This type of approach was first developed by Goldin and Menon [8][9], who employed the LEM to construct a database of mean species properties as a function of mean mixture fraction, mixture fraction variance and scalar dissipation. That type of parameterization is very similar to what is used for the laminar flamelet turbulent combustion model [2]. Goldin and Menon [9] applied this methodology for *a priori* comparisons of species and temperature pdfs with experimental data. That study demonstrated the excellent agreement between LEM predicted pdfs and those obtained from experiments for hydrogen-air and methane-air jet flames. That study also demonstrated the superiority of the LEM approach compared with the assumed pdf formulation that is used within the flamelet model.[2] Goldin and Menon [8] also applied this approach to the RANS predictions of a hydrogen-air jet flame and obtained excellent results compared to experimental data for mean species and mixture fraction. Good predictions of mean temperature and pollutant formation for Sandia flames D and F were also achieved by Goldin and Raman [10] using the parameterized LEM approach. Sankaran, et al. [11] developed a parameterized LEM combustion model as a function of mean mixture fraction, scalar dissipation and turbulent Reynolds number and made *a priori* comparisons with experimental scatter plot data for species and temperature for a $CH_4/H_2/N_2$ jet flame. Sen and Menon [12] generalized this approach to develop a LEM parameterized model for an 11 species – 22 reaction step mechanism for H_2/CO – air combustion. In their approach, the filter species production rates for the mechanism were parameterized in terms of mean temperature, species, species gradient and subgrid Reynolds number. Sen and Menon [12] applied this model to predict local extinction and re-ignition in a temporally evolving jet simulation and produced good results compared to DNS data.

LEM parameterized models are very powerful and computationally efficient, making them an excellent choice for routine application of LES to engineering design and analysis of combustor and augmentor flows. However, current LEM formulations are deficient from the perspective that they *do not* include the effect of large or resolved scale strain. This results from that fact that current LEM formulations assume uniform mean flow within the subgrid. Consequently, these formulations cannot capture the effect of resolved scale strain on the subgrid combustion. Some previous LEM parameterized models [11][12] attempted to include resolved scale strain effects within their formulations by initializing the LEM simulations used to generate the models with strained laminar flame solutions. However, these strain effects were only contained within the initial conditions and were not maintained during the LEM simulations because these formulations assumed uniform mean flow within the LEM. The generalized LES-LEM [3][4] formulation which directly employs stochastic simulations using the LEM within each LES subgrid cell also does not account for the effect of resolved scale strain on the subgrid for the same reason. This is also true for the pdf evolution equation method [5] because the subgrid mixing models used in that approach do not account for mean strain either.

The lack of accounting for resolved scale strain on the subgrid for both the LEM and pdf evolution equation methods may result in an underprediction of local flame extinction, for example, in the vicinity of the high strain region between two counter rotating vortices. To resolve this deficiency, the objective of this research is to develop a LEM formulation that will account for mean or resolved scale strain on the subgrid flow. This is accomplished by developing a fully coupled LEM/counter flow solver that may be used to predict the behavior of turbulent counter flow flames under the influence of mean strain. With this new formulation, statistics may be generated to close the filtered LES equations within a parameterized LEM model that directly includes the resolved scale strain as an input parameter. The resulting model will be computationally inexpensive and directly account for both resolved and unresolved strain effects on the extinction and ignition behavior of the subgrid flame.

This paper describes the development of this fully coupled LEM/counter flow (LEM-CF) formulation to predict turbulent counter flow flames. This paper also describes the application of this methodology to augmentor like conditions, and illustrates how this approach may be used to generate a computationally inexpensive run-time model for LES.

The following section of this paper first describes the basic LEM for application to homogeneous turbulence. Next, a counter flow formulation to predict the mean velocity field is presented that was developed to be amenable to coupling with the stochastic LEM. A description of modifications to the basic LEM that are required to apply the model to the counter flow configuration is then presented, along with a description of the strategy used to couple the LEM and counter flow solvers. Results are then presented for the application of this unique LEM-CF formulation to augmentor-like conditions. A methodology is also described to generate a parameterized LEM combustion model for those conditions. Conclusion and recommendations then follow.

LINEAR-EDDY MODEL SUMMARY

The linear-eddy model is a stand-alone turbulent combustion model for the simulation of flame evolution in isotropic turbulence under constant pressure conditions. The model is designed to separately treat two fundamental physical processes that describe the evolution of chemical species in turbulent flames. In doing so, an accurate picture of the interaction of the turbulence and chemistry may be obtained. The two processes treated within the model are molecular diffusion and turbulent convective stirring. Molecular diffusion is treated deterministically by the numerical solution of the species and temperature diffusion equations, which include the

effects of chemical reactions and volumetric expansion. Turbulent stirring, however, is modeled stochastically by a series of instantaneous rearrangement events of the species and temperature fields. Due to the isotropic nature of the model, it is formulated in only one spatial dimension. The 1-D LEM scalar domain has been interpreted as a time varying space curve that is aligned with the maximum scalar gradient within the flow. For this 1-D domain, the strategy employed within the model is to resolve *all* relevant fluid mechanical length scales as in direct numerical simulation. As a result, the reaction rate source terms in the species and temperature equations appear in *closed* form and do not require additional modeling. Also, because the model is formulated in 1-D, resolving all the length scales of the flow is computationally tractable. The smallest length scales that must be resolved are the Kolmogorov microscale for momentum transport and the Bachelor scale for species diffusion.

The model equations for the influence of molecular diffusion and chemical reactions on the time evolution of the species mass fraction, Y_k, and temperature, T, fields within the LEM 1-D spatial coordinate, x, are given by:

$$\frac{\partial Y_k}{\partial t} = -\frac{1}{\rho}\frac{\partial(\rho Y_k U_k)}{\partial x} + \frac{\dot{\omega}_k}{\rho} \tag{1}$$

$$\frac{\partial T}{\partial t} = \frac{1}{\rho c_p}\frac{\partial}{\partial x}\left(\lambda\frac{\partial T}{\partial x}\right) - \frac{1}{c_p}\sum_{k=1}^{K}(c_{p,k}Y_k U_k)\frac{\partial T}{\partial x} - \frac{1}{\rho c_p}\sum_{k=1}^{K}(h_k\dot{\omega}_k) \tag{2}$$

where ρ, λ and c_p are the mixture density, thermal conductivity and constant pressure specific heat, respectively. Also, U_k, $\dot{\omega}_k$, $c_{p,k}$ and h_k are the kth species diffusion velocity, chemical production rate, constant pressure specific heat and enthalpy, respectively. The species diffusion velocities, U_k, may be modeled using any level of sophistication desired, from constant or mixture averaged diffusion coefficients to the solution of the multicomponent diffusion equation. Since the model formulation explicitly includes molecular diffusion, the LEM directly captures Schmidt number (*Sc*) and differential diffusion effects. No other mixing model formulation has this capability.

Turbulent convection within the linear-eddy model is treated as a series of randomly located instantaneous rearrangement events of the species and temperature fields. These rearrangement events correspond to mixing induced by turbulent eddies. The eddy size l and frequency λ_M of these events are determined based on Kolmogorov scaling for high Reynolds number flow. Given values for l and λ_M, a mapping procedure called the *triplet map* [7] is used to rearrange the distribution of the scalar fields. This mapping was developed by Kerstein [7] to simulate the effect of small scale turbulent stirring on diffusion layers. The mapping generates discontinuous (turbulent) fluid motion and causes a random walk of the fluid particles. The effect of this mapping procedure is to increase the local scalar gradient, as is characteristic of the action of turbulent eddies on scalar fields. The mapping procedure is designed to satisfy species and energy conservation and does not introduce any mass or thermal diffusion. The triplet mapping eddy size l is chosen randomly from a power-law distribution $f(l)$ within the range $n_K < l < L$, where n_K and L are the Kolmogorov and integral scales of turbulence, respectively. Relationships [6] for $f(l)$ and the frequency parameter λ_M are derived by equating the diffusivity of a random walk of a fluid particle under the influence of the mapping procedure with high Reynolds number scaling for turbulent diffusivity. As a result, these relationships are a direct function of the turbulent Reynolds number, $Re_L = u'L/\nu$.

The LEM does not assume scale separation between the flame thickness and the turbulent mixing scales [2]. As a result, the model is applicable to all flame regimes of turbulent combustion. This feature of the model distinguishes it from other mixing model formulations.

The basic LEM model may be applied to a variety of flow configurations through the specification of appropriate initial and boundary conditions, as well as application-specific processes needed to supplement the basic convection and diffusion algorithms. This includes the specification of the mean flow, since the LEM does not directly account for mean flow effects, including large scale strain. The capabilities of the LEM model have been demonstrated for flows that include mixing in grid turbulence, reacting mixing layers, mixing and reacting jets, mixing in homogeneous turbulence, and for premixed flame applications. Calhoon [13] presents a comprehensive review of the model's capabilities.

To apply mean flow strain effects to the LEM, the model may be formulated for the counter flow configuration. This requires a methodology to specify the effect of the mean velocity on the LEM stochastic particles. This is accomplished by coupling the model with a counter flow solver for the mean flow variables, including the velocity. The following section describes the development of a specialized counter flow solver that was coupled to the LEM.

COUNTER FLOW FORMULATION

A specialized counter flow formulation and solver was developed for coupling with the LEM. This counter flow solver provides the mean velocity field to the LEM solver, while the LEM solver provides heat release effects back to the counter flow solver. The LEM solver requires the mean velocity in turbulent flow. Therefore, the counter flow solver must include a turbulence model for momentum transport. Also, the counter flow formulation must be unsteady to account for the time evolution of the LEM statistics, and to account for unsteady effects such as autoignition. The counter flow formulation employed in this study was based on the low Mach number formulation of Im, et al. [14]. As described by Im, et al. [14], the low Mach number assumption decouples the axial momentum equation from the system, and decouples the effect of the hydrodynamic pressure on heat release from combustion. The system of equations then reduces to the continuity, radial momentum, species conservation, and temperature equations, along with a compatibility relation for the pressure eigenvalue [14]. This formulation was modified by replacing the temperature equation with an equation for the internal energy that was derived using the low Mach number assumption. The

internal energy equation does not include any chemical source terms that must be modeled for turbulent flow.

Reynolds averaging was then applied to these equations for application to turbulent flow. This resulted in a collection of unclosed terms associated with the averaging of the convection, diffusion and chemical source terms. All turbulent fluctuations within diffusion related terms were neglected. Terms associated with averaged chemical source terms will be modeled using the LEM combustion formulation. The remaining unclosed terms are the turbulent momentum, species and thermal transport terms. These terms are modeled using the turbulent viscosity and gradient diffusion hypotheses [15], with the eddy viscosity (μ_T) specified in terms of the mean density, velocity fluctuation (u') and integral length scale of turbulence (L). This representation of the eddy viscosity may in turn be written in terms of the turbulent Reynolds number, Re_L, as,

$$\mu_T = \bar{\rho} u' L = \bar{\mu} Re_L \tag{3}$$

where the overbar represents Reynolds averaging. The Reynolds number in this equation is the same one specified for the LEM turbulent stirring algorithm described earlier.

With this turbulence model formulation, the final form of the continuity, radial momentum, species conservation, and internal energy equations are,

$$\frac{\partial \rho}{\partial t} + \frac{\partial (\rho u)}{\partial x} + 2\rho V = 0 \tag{4}$$

$$\rho \frac{\partial V}{\partial t} + \rho u \frac{\partial V}{\partial x} + \rho V^2 - \frac{\partial}{\partial x}\left((\mu + \mu_T) \frac{\partial V}{\partial x} \right) + \Lambda = 0 \tag{5}$$

$$\rho \frac{\partial Y_k}{\partial t} + \rho u \frac{\partial Y_k}{\partial x} + \frac{\partial}{\partial x}\left(\rho Y_k U_k \right) - \frac{\partial}{\partial x}\left(\frac{\mu_T}{Sc_T} \frac{\partial Y_k}{\partial x} \right) - \overline{\dot{\omega}_k} = 0 \tag{6}$$

$$\begin{aligned} &\rho \frac{\partial e}{\partial t} + \rho u \frac{\partial e}{\partial x} + p_0 \left(\frac{\partial u}{\partial x} + 2V \right) \\ &- \frac{\partial}{\partial x}\left((\lambda + \frac{\mu_T}{\mathrm{Pr}_T} c_v) \frac{\partial T}{\partial x} \right) \\ &+ \frac{\partial}{\partial x}\left(\rho \sum_{k=1}^{K} h_k Y_k U_k \right) = 0 \end{aligned} \tag{7}$$

$$\frac{\partial \Lambda}{\partial x} = 0 \tag{8}$$

where ρ is the density, u is the axial velocity, V is the normalized radial velocity [14], e is the specific internal energy [16], and Λ is the pressure eigenvalue [14]. In these equations all the overbars and symbols that denote Reynolds and Favre quantities have been dropped for clarity. The parameters Sc_T and Pr_T are the turbulent Schmidt and Prandtl numbers and were specified as $Sc_T = Pr_T = 0.7$, consistent with low speed jet flow experiments. The only unclosed terms in this system of equations are the chemical production terms in Eqn. (6). This closure issue will be addressed using the LEM turbulent combustion modeling formulation to be described in the next section. Also, these equations are supplemented with the low Mach number equation of state [14] and the definition of the internal energy in terms of temperature and species mass fractions.

The boundary conditions for this system of equations are described by Im, et al. [14] and are not repeated here for brevity. The spatial discretization procedure used for these equations also followed Im, et al. [14]. These equations are advanced in time using a first order implicit method, which includes sub-stepping to converge the pressure eigenvalue at each time step.

The mathematical formulation and the numerical implementation of this system of equations were verified by a comparison of results for steady-state, laminar, nonreacting and reacting flows with those of a well developed steady-state solver based on the work of Smooke, et al. [17]. For application to turbulent flows, the LEM is required to close the equation system. The next section describes the application of the LEM to the counter flow configuration, and the strategy used to couple the LEM and counter flow solvers.

LEM / COUNTER FLOW (LEM-CF) FORMULATION

The basic LEM model formulation must be modified to apply it to the counter flow configuration. Additionally, a strategy must be defined to couple the LEM with the counter flow solver. These two issues are addressed in the following sub-sections.

LEM Application to the Counter Flow Configuration

To apply the LEM to the counter flow configuration requires the inclusion of mean convection on the species and temperature stochastic particles, particle removal at the stagnation point, and the inclusion of volumetric expansion due to heat release. To account for mean convection, the stochastic particles must be transported in space due to the mean counter flow axial velocity. This is accomplished as follows. First, the LEM particles are initially distributed on equal intervals between the counter flow jet nozzle exit planes. At these particle locations, the mean axial velocity from the counter flow solver is interpolated to associate a mean velocity with each LEM stochastic particle. Second, the LEM particles are convected within a Lagrangian formulation using a fourth order Runga-Kutta solver, with the velocity updated at the sub-step locations through interpolation. The LEM diffusion equations (Eqns. (1) and (2)) are then solved with an implicit method.

As the LEM stochastic particles convect along the counter flow domain, new LEM particles enter the domain at the jet boundaries and particles collect around the stagnation point. To maintain a constant number of LEM particles within the simulation, particles whose spatial location falls within the range,

$$x_{u=0} - \delta/2 \le x \le x_{u=0} + \delta/2 \tag{9}$$

are removed from the simulation, where $x_{u=0}$ is the stagnation plane, and δ is the initial equal particle distribution interval. This particle removal procedure is justified because, as with all LEM implementations, the diffusion fields are *fully* resolved as in a direct numerical simulation. As a result, no information is lost in this process since the original equal particle distribution, δ, fully resolved the flow. The initial particle spacing was set equal to one-sixth the width of the Kolmogorov microscale, as is typical for LEM implementations.

As mentioned earlier, the LEM assumes constant thermodynamic pressure. With this assumption, volumetric expansion due to heat release must be accounted for. Typically, LEM implementations must explicitly account for this effect because the model *does not* include mean convection. In this case, the LEM grid cells are explicitly expanded based on density differences due to chemical heat release [13]. This expansion algorithm *implicitly* induces mean flow convection resulting from heat release. For the present application to the counter flow configuration, however, mean convection is *explicitly* accounted for as described earlier. As a result, the mean velocity field accounts for volumetric expansion through the solution of the continuity equation in the counter flow solver. Consequently, volumetric expansion does not need to be explicitly implemented within the LEM diffusion solver as applied to the counter flow configuration.

As discussed earlier, turbulent convection within the LEM is treated as a series of randomly located instantaneous rearrangement events of the species and temperature fields. These rearrangement events correspond to mixing induced by turbulent eddies. The eddy size l and frequency λ_M of these events are determined based on Kolmogorov scaling for high Reynolds number flow [6]. The inputs for the turbulent stirring algorithm are the integral scale of turbulence, L, and the turbulent Reynolds number, Re_L. For the counter flow configuration, Re_L is defined in terms of the axial velocity fluctuation by,

$$Re_L = \frac{u'L}{(\nu_{FUEL} + \nu_{OXI})/2} \tag{10}$$

where the kinematic viscosity in this relationship is taken as the average between the two jet exit conditions (i.e., ν_{FUEL}, ν_{OXI}). The value of the viscosity used in Eqn. (10) may be specified in an arbitrary manner as long as the *same* value is used for both the LEM sub-model and within a LES case. Consequently, the average of the boundary values was chosen because it is well defined and independent of heat release within the simulation. For the counter flow configuration, changes in Re_L may be accomplished by increasing the diameter of the fuel and oxidizer jets, assuming both jets have the same diameter, D, and/or by changing L. To relate the LEM Reynolds number and length scale to a physical counter flow configuration, the following assumptions were made:

1) L is equal to the jet separation distance, X_L.
2) For turbulent counter flow conditions, the jets exhaust from fully developed turbulent pipe flows.
3) L is also equal to the centerline mixing length, l_T, for fully developed turbulent pipe flow.
4) u' is equal to the centerline axial velocity fluctuation for fully developed turbulent pipe flow.
5) The jet momenta are assumed equal.

The first assumption is consistent with the application of the LEM to large-eddy simulation (LES) of turbulent reacting flows. For LES, the LEM length scale is set equal to the LES filter width, Δ, or the maximum spatial extent of the subgrid domain. For the counter flow configuration, the maximum spatial extent is the jet separation width X_L. The second assumption is also reasonable for turbulent counter flow configurations. This assumption is also needed because the LEM stirring relationships assume high Reynolds number flow, as mentioned earlier. With the second assumption, the third assumption follows since the maximum turbulent length scale in pipe flow occurs at the centerline [18]. The fourth assumption regarding the axial velocity fluctuation is also consistent with the assumption of turbulent pipe flow. The last assumption is typical for counter flow models and is used to establish the stagnation plane in the center between the two jet exhausts. With these assumptions and the scaling relationships for fully developed pipe flow, the jet velocities (u_{FUEL}, u_{OXI}), jet separation distance (X_L) and diameter (D) may be determined given the jet thermodynamic conditions, turbulent Reynolds number (Re_L), and the mean strain rate ($<a>$), where $<a>$ is defined by,

$$< a >= \frac{|u_{FUEL}| - |u_{OXI}|}{X_L} \tag{11}$$

Appendix I presents a derivation of the relationships and methodology required to determine these quantities. From these relationships, the jet diameter is given by,

$$D = \left[\frac{Re_L(\nu_{FUEL} + \nu_{OXI})/2}{(0.07)M_0^{1/2} C_0^{1/2} (u_B^{7/8} \nu^{1/8})} \right]^{8/7} \tag{12}$$

where M_0 and C_0 are experimental correlations and u_B is the maximum jet bulk velocity (see Appendix I). Given the diameter and jet velocities, the jet Reynolds numbers are then given by,

$$Re_{fuel} = \frac{u_{FUEL} D}{\nu_{FUEL}},\ Re_{OXI} = \frac{u_{OXI} D}{\nu_{OXI}} \tag{13}$$

With these relationships, a connection between a LEM/counter flow simulation and a laboratory set-up for a turbulent counter flow flame may be established.

The final consideration for applying the LEM turbulent stirring algorithm to the counter flow configuration concerns the method in choosing the location where a stirring event will occur. Typically, the LEM is formulated for homogeneous turbulence with no mean flow so that the LEM domain is periodic. As a result, a stirring event is chosen randomly with a uniform probability along the entire domain irrespective of the eddy size. However, for the counter flow configuration, the LEM domain is spatially confined to the jet separation distance. The event location must then be restricted based on the event eddy size so as to prevent the transport of fluid outside the domain boundaries. Given this restriction, a stirring event is implemented by randomly choosing the event location on the counter flow domain with uniform probability, excluding locations that would result in an overlap of the domain boundaries. This implementation is the same as the one used by Menon and Calhoon [3] for LES-LEM simulations of reacting shear layers. In that study, the LEM domain within each LES subgrid contained an inflow and an outflow boundary, thereby necessitating this type of stirring implementation. For the counter flow configuration, limiting

the stirring events in this manner is equivalent to excluding back flow into the jet nozzles, which is a reasonable assumption.

LEM / Counter Flow Solver Coupling Strategy

To enable heat release from the LEM simulation to affect the mean velocity field, a strategy was developed to fully couple the LEM and counter flow solvers. This strategy is outlined below:

1) The counter flow solver, which includes the turbulence model for momentum transport, provides the mean axial velocity, u, to the LEM solver.
2) Scalar statistics are calculated from solution realizations of the LEM solver given u.
3) The LEM mean scalar statistics for the species mass fraction and density are provided to the counter flow solver to enable the velocity field to be determined.

With this coupling strategy, the mean species transport equations within the counter flow formulation (Eqn. (6)) do not need to be solved. This eliminates the need to directly model the mean chemical source terms in these equations, though they could be directly specified using the LEM. For statistically steady-state problems, the density time derivative in the counter flow continuity equation (Eqn. (4)) is also neglected. However, this term may be retained for problems that are unsteady in the mean, with this term being calculated directly from the evolution of the LEM statistics. For the LEM statistics, mean variables are calculated over an averaging window of typically the last 1000 realizations of the solution. These realizations are collected on a frequency that roughly corresponds to the LEM stirring frequency. This data collection frequency was chosen so that the statistics could adequately converge. Averaging over a significantly higher frequency (such as the LEM diffusion step frequency) resulted in poorly converged statistics. Convergence of the LEM statistics for the 1000 realizations was verified by a comparison of the mean axial velocity field to a simulation that employed 2000 realizations. The two simulations produced very close results for the mean axial velocity in both space and time as the counter flow solution evolved.

With the LEM mean statistics, the counter flow solver is employed to recalculate the mean axial velocity in response to heat release effects within the LEM. At each counter flow solution step, the counter flow equations are sub-iterated to ensure the convergence of the pressure eigenvalue and mass conservation. This coupling strategy is very robust so that converged statistics may be obtained given practically any initial condition for the velocity and temperature fields that satisfies the boundary condition. As a result, LEM-CF simulations are initialized with hyperbolic tangent like axial velocity and mixture fraction profiles. With this profile for mixture fraction, the species and temperature are initialized with equilibrium values. Initializing the simulations in this manner results in large initial oscillations of the pressure eigenvalue in order to adjust the velocity fields to conserve mass. These large oscillations damp out quickly (within 50 counter flow solution steps) so that the pressure eigenvalue is within a relatively small percentage of the final converged value.

With a description of the LEM-CF formulation now complete, the next section presents the results from the application of this methodology to augmentor-like conditions, and describes the approach to using this methodology to build a subgrid combustion model for LES.

APPLICATION OF LEM-CF TO AUGMENTOR CONDITIONS

The LEM-CF formulation was applied to augmentor-like conditions to investigate the model characteristics, and to illustrate the methodology used to generate a parameterized LEM combustion model that could be deployed within a CFD flow solver. The thermodynamic conditions for this investigation are listed in Table I. The oxidizer stream consisted of vitiated air at a temperature of 1196 K and the fuel stream consisted of an ethylene surrogate at a temperature of 339 K. The pressure was 57.56 psi. A reduced ethylene chemical mechanism [19] was used to represent the chemistry. This mechanism includes 19 species and 15 global reaction steps. This mechanism was developed from a larger detailed mechanism using the quasi-steady state assumption for selected minor species [19]. This mechanism has been validated for ignition delay times, premixed laminar flame speeds, and opposed flow diffusion flame properties and extinction.

Table I: Counter flow jet boundary conditions.

Vitiated air	T = 1196 K, F/O = 0.010798
Surrogate fuel	Ethylene, T = 339 K

The two primary parameters that were varied to generate the LEM parameterized model were the turbulent Reynolds number (Re_L) and mean strain rate ($\langle a \rangle$). As mentioned earlier, given the Reynolds number and mean strain rate, along with the flow thermodynamic conditions, the counter flow jet separation distance (X_L), jet diameter (D), jet exhaust velocities (u_{FUEL}, u_{OXI}), and jet Reynolds numbers (Re_{FUEL}, Re_{OXI}) may be determined.

The parameter space for the LEM statistics generated from the LEM-CF simulations covered a range of values for the mean strain rate, $\langle a \rangle$, and Re_L. For the strain rate, the maximum value of $\langle a \rangle$ was based on the laminar flow extinction limit value of ~ $1.70 \times 10^{+4}$ 1/sec. Given this value, ten strain rate values were chosen for each Reynolds number in the range $1.06 \times 10^{+3} \leq \langle a \rangle \leq 1.75 \times 10^{+4}$ 1/sec. For the Reynolds number, the values chosen were Re_L = 0, 10, 50, 100, 1000. The value of Re_L = 1000 is very high and represents intense mixing. Given these values of strain rate and Reynolds number, Table A1 (in Appendix II) defines the simulation matrix for the statistics generation process. The table lists the turbulent length scale (L), jet velocities (u_{FUEL}, u_{OXI}), jet diameter (D), and jet Reynolds numbers (Re_{FUEL}, Re_{OXI}) for each case. Also, recall from the assumptions listed earlier that $L = X_L$. From this table it may be observed that for a specified Reynolds number the values of L, D and the jet velocity all vary with varying strain rate. Observe for the turbulent cases that increases in strain rate are achieved by reducing the separation distance (L) and by increasing the jet velocities. Also, for a

specified Re_L, the jet Reynolds numbers are constant for all strain rates. The strain rate values for each Reynolds number are also clustered around the extinction value, as will be discussed later. The LEM particle spacing for each case listed in Table A1 also resolved the Kolmogorov microscale using at least six points, as it typically employed for the LEM.

From the simulation results for these cases, the following observations may be made. First, for the laminar flow cases (Cases 1 – 10), the simulations burn for all strain rates except Cases 9 and 10, which are at or beyond the extinction limit. As the strain rate increased for these cases, the peak temperature, major product, and OH mass fraction values all decreased, as expected. However, for some radical species such as O, as the strain rate was increased, higher peak values were realized as the flames were pushed further away from equilibrium up to some intermediate strain rate. Further increases in $<a>$ beyond this value then suppressed O production until extinction was reached.

The second observation from these LEM-CF simulations that may be drawn is that for the turbulent cases, the mean flame structure is broad with respect to the jet separation distance X_L. This result is a consequence of the assumption that the turbulent integral scale is equal to the jet separation distance, as was discussed earlier. Recall that this assumption was employed to be consistent with the application of the LEM within LES codes, where L is set equal to the subgrid filter scale, which is the largest extent of the subgrid domain.

The third observation from these simulations is that for all turbulent cases (e.g., Cases 11 – 50), flame extinction occurred prior to a mean strain rate value of $<a>$ = 6.67E+03 1/sec for all Reynolds numbers. The extinction limit varied with Re_L, but was within the range $2.54\text{x}10^{+3} \le <a> \le 6.67\text{x}10^{+3}$ 1/sec. The last column in Table A1 indicates whether global extinction occurred for each case. Global extinction was defined as the strain rate where the flame on the LEM computational domain extinguished for *eight* different realizations of the model, where each realization was initialized with a different random seed. As a result, the evolution of the instantaneous flame structure for each realization followed a different convergence path and yielded a different possibility of extinction occurring. At low strain rates, all realizations would burn. As the strain rate was increased, some of the realizations would extinguish while others would continue to burn. As the strain rate approached the global extinction limit, a larger number of realizations would extinguish. The strain rate for which all the realizations extinguished was therefore defined as the global extinction limit. The extinction limit predictions were also verified for LEM particle spacing convergence by decreasing the spacing by a factor of 2 and 3 for selected cases. The predicted limits were unaffected by the grid distribution, thereby verifying the LEM computational resolution.

To illustrate an extinction event within the LEM, Figure 1 presents instantaneous temperature profiles for Re_L = 50 and $<a> = 3.69\text{x}10^{+3}$ 1/sec at three instants in time. From this figure, note that at the early times t_1 and t_2, the temperature profiles exhibit locally high values larger than 2000 K. By the time t_3, however, the flame is entirely extinguished (as noted in the figure) with local temperatures no higher than the vitiated air temperature. However, at this strain rate, some of other simulation realizations continued to burn so that global extinction was not achieved until $<a> = 5.09\text{x}10^{+3}$ 1/sec as noted in Table II, which lists the extinction limits as a function of Reynolds number. For this value of strain rate, the laminar flow case is well below the extinction value. Similarly for the other Reynolds number cases, extinction occurred well below the laminar flame values as illustrated in Table II. This table shows that the global extinction limit initially drops rapidly as Re_L is increased, and then appears to approach an asymptotic value at higher Re_L. These results illustrate that the inclusion of small scale turbulent strain significantly reduces the extinction limit for a fixed value of mean large scale strain rate $<a>$. This is not a surprising result, but a very important one that illustrates the utility of the LEM-CF methodology to capture this type of behavior. Currently, there is no other way to predict this type of behavior besides a full, 3-D DNS. However, DNS would likely be intractable at these high jet Reynolds numbers (Table A1).

Table II: Extinction Limits as a Function of Reynolds Number

Re_L	$<a>_{ext} \times 10^{-3}$
0	17.01
10	6.67
50	5.09
100	3.69
1000	2.54

The extinction behavior illustrated in Figure 1 cannot be accurately captured by the flamelet combustion model or the pdf evolution equation approaches because neither of these methods resolves the flame structure. For the flamelet model, strain rate effects and extinction are modeled in terms of the laminar flow flame properties averaged over an assumed shape pdf for mixture fraction. For pdf methods, turbulent strain and extinction effects are modeled with a single point statistical model for turbulent mixing that does not resolve the microscale flame structure.

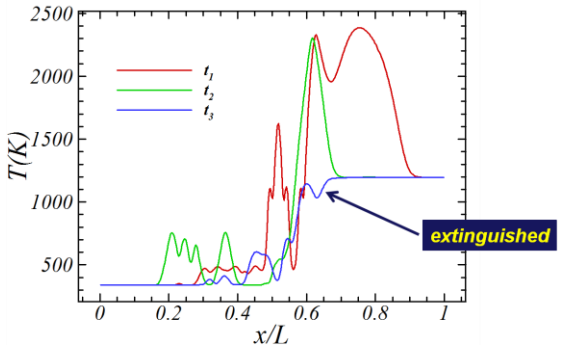

Figure 1. Instantaneous temperature profiles for a turbulent counter flow flame at Re_L = 50 and $<a>$ = 3695 sec^{-1}.

Below the extinction strain rate for the turbulent cases of Table A1, mean flame properties may be computed from the LEM-CF simulations. For example, Figure 2 presents the mean axial velocity for Re_L = 50 for different values of mean strain rate. This figure plots the mean velocity as a function of x/L.

In this figure it is apparent that as the strain rate increases, the velocity gradient at the stagnation point also increases. The gradient $\partial u / \partial x$ is actually higher than shown in Figure 2 because the length scale L decreases as the strain rate increases, as shown in Table A1. The mean velocities plotted in this figure also include the effects of mean heat release from the LEM through the LEM-CF coupling strategy described earlier. For the cases shown in Figure 2 that are well below the extinction strain rate (i.e., $\langle a \rangle$ = 1056, 1681 and 2537 1/sec), the axial velocity profiles show a slight overshot of the boundary values due to heat release effects. For $\langle a \rangle$ = 3695 1/sec case, which is close to the extinction limit and partially extinguished (as noted earlier), the reduced level of heat release results in a monotonic axial velocity profile.

Heat release within the LEM statistics is illustrated in Figure 3, which presents the Favre mean temperature along the jet axis as a function of strain rate. From this Figure, the reduced extent of the spatial domain (L) with increasing $\langle a \rangle$ is evident, as noted in Table A1. Also note that the peak mean temperature gradually drops as $\langle a \rangle$ is increased until the extinction limit is approached. Beyond $\langle a \rangle$ = 2537 1/sec, the peak temperature rapidly drops until global extinction occurs. This may also be seen in Figure 4, which re-plots the results of Figure 3 as a function of x/L. From this figure, the effect of the strain rate on the temperature field is small for $\langle a \rangle$ = 1056 and 1681 1/sec. Beyond these values, the peak temperature progressively drops off. The temperature profiles in this figure also exhibit an inflection point at $x/L \sim 0.5$, which is the stagnation plane. This behavior is a result of a mild inflection point in the axial velocity profile when heat release is present.

Mean product mass fractions for these cases closely parallel the results for mean temperature seen in Figures 3 and 4. For example, Figure 5 presents mean CO_2 mass fraction as a function of x/L. As seen in this figure, the drop in peak values with increasing strain and the inflection point at the stagnation plane prior to extinction closely follow the trends of Figure 4. However, the peak CO_2 values in Figure 5 are more sensitive to the strain rate, particularly at low values, than were the temperature peaks in Figure 3. Regarding the radical species, Figure 6 presents mean O mass fraction for these cases. From this figure, the peak O mass fraction value increases with strain rate until a maximum is reached at $\langle a \rangle$ = 2537 1/sec. At higher strain rates, the peak value quickly drops until extinction is approached. This behavior for O mass fraction is similar to what was observed for the laminar cases. However, the peak O mass fraction occurred at a much higher mean strain rate for laminar flow. This illustrates that adding turbulent microscale strain to the flow more rapidly pushes the flame to nonequilibrium and global extinction.

OH mass fraction results for the LEM-CF cases (Figure 7) behave very similar to the O mass fraction results plotted in Figure 6. Peak OH mass fraction increases with strain rate to a maximum value at $\langle a \rangle$ = 2537 1/sec, and then decreases with further increases in $\langle a \rangle$ until extinction is approached. For the laminar case, however, the peak OH mass fraction *continuously* decreases as strain rate is increased. This may be seen in Figure 8 which plots OH mass fraction along the jet axis as a function of strain rate for the laminar flow cases. This difference in the behavior of the maximum OH mass fraction between the laminar and turbulent flow cases illustrates the following point. The interaction of the microscale turbulence with the flame structure fundamentally alters the nature of the nonequilibrium processes occurring within the flame. That is, the turbulence not only hastens the onset of nonequilibrium effects and extinction, but it also alters the chemical kinetic pathways that these effects follow on the way to extinction. This illustrates the capability of the LEM-CF to fundamentally capture the interaction of microscale turbulence with the flame structure. Other turbulent combustion model formulations, such as the laminar flamelet model [2], that assume scale separation between the flame thickness and Kolmogorov microscale cannot capture this type of behavior. For example, a laminar flamelet model table for this case would be based on the laminar flow result in Figure 8, averaged over an assumed pdf of mixture fractions. As a result, such a flamelet model table could *never* capture the behavior seen in Figure 7 for the turbulent flow case. Additionally, other parameterized models [8]–[12] based on the LEM formulated for homogenous turbulence also could not capture the effects seen in Figure 7. Those formulations do not include mean strain effects and would produce results similar to the lowest strain rate result in Figure 7. The only way to produce higher OH values for those models would be to increase the microscale strain by increasing the Reynolds number. However, increased microscale strain with increased Re_L will not necessarily increase nonequilibrium OH values, as will be demonstrated later.

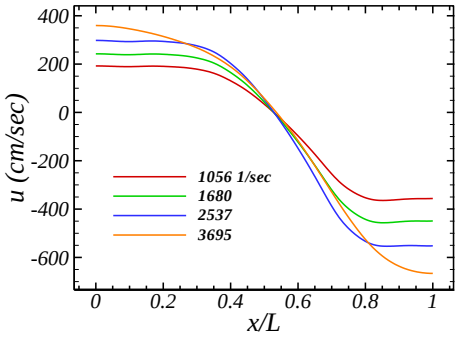

Figure 2. Mean axial velocity as a function of strain rate at Re_L = 50.

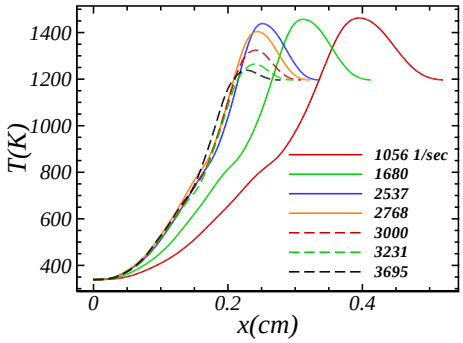

Figure 3. Mean temperature variation with strain rate plotted as a function of x at Re_L = 50.

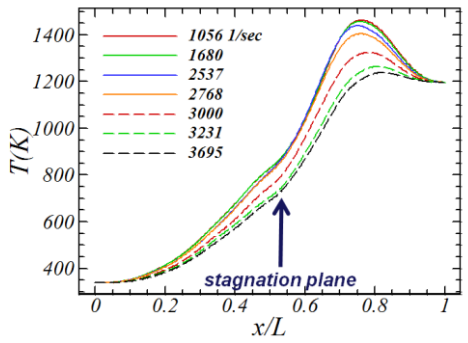

Figure 4. Mean temperature variation with strain rate plotted as a function of *x/L* at Re_L = 50.

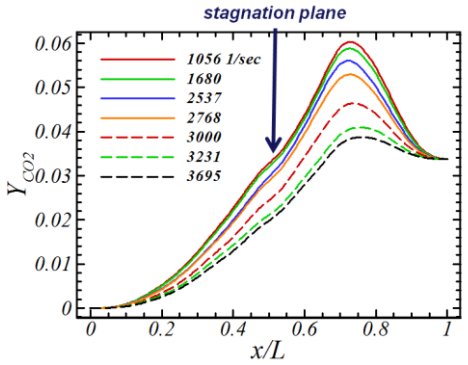

Figure 5. Mean CO_2 mass fraction variation with strain rate plotted as a function of *x/L* at Re_L = 50.

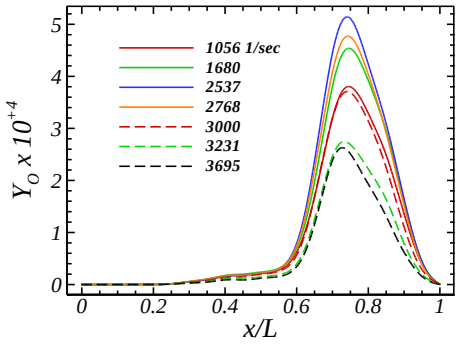

Figure 6. Mean O mass fraction variation with strain rate plotted as a function of *x/L* at Re_L = 50.

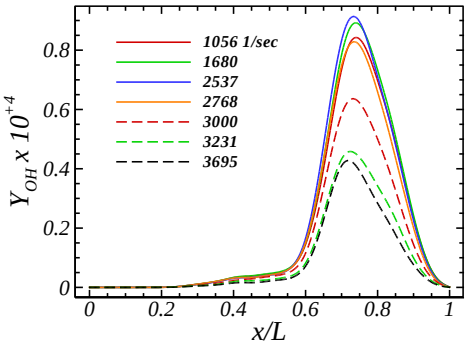

Figure 7. Mean OH mass fraction variation with strain rate plotted as a function of *x/L* at Re_L = 50.

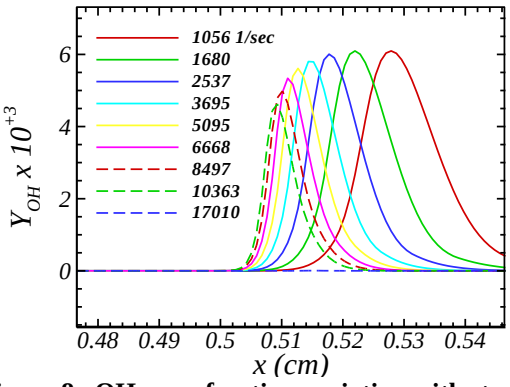

Figure 8. OH mass fraction variation with strain rate plotted as a function of *x* for laminar flow.

The previous figures have illustrated the effect of strain rate on the flow at a constant Reynolds number. The effect of Reynolds number on the statistics may be observed by examining a series of results at constant strain rate. For example, Figure 9 presents Favre mean temperature results for Re_L = 10, 50, 100 and 1000 at a strain rate of <*a*> = 1056 1/sec. At this low strain rate, the instantaneous flame structure is the closest to equilibrium. In this figure, the mean temperature is plotted with respect to the normalized coordinate *x/L* as in Figure 4. From Figure 9, the following trends may be observed. First, increases in Re_L substantially reduce the peak flame temperature. Second, the results for all cases show an inflection point in the data at the stagnation plane. Third, the location of peak mean temperature moves further away from the oxidizer jet (*x* = 0) as Re_L is increased, except for the Re_L = 1000 case. These trends for the temperature were also seen for the major product species, as illustrated in Figure 10 for Favre mean CO_2 mass fraction. These same trends consistently occurred at the other strain rates as well.

The reduction in peak values of temperature and major product species with increased Reynolds number also occurs for the radical species. For example, Figure 11 and 12 present Favre mean O and OH mass fraction profiles for these Reynolds numbers. As seen in both of these figures, the peak mean values for both of these species decrease as Re_L is increased. This same trend was observed for the other strain rates as well. These results illustrate that increases in the microscale strain through larger values of Reynolds number alone cannot produce a high enough degree of nonequilibrium to cause an increase in these radical species, as seen in Figures 6 and 7 when the strain rate was increased. Consequently, other parameterized LEM models that do not include mean strain effects cannot capture the higher radical levels seen in Figures 6 and 7, as mentioned earlier.

The reduction in the maximum values of temperature, major species, and radical species seen in Figures 9 – 12 for increased Reynolds number appear to be primarily a result of mixture fraction fluctuations. Figure 13 presents mixture fraction fluctuation intensity at <*a*> = 1056 1/sec for the Re_L = 10, 50, 100 and 1000 cases. As seen in this figure, the fluctuations dramatically increase with Reynolds number. An examination of instantaneous temperature profiles for these cases showed that the peak temperatures realized within the flow were close to the laminar case value. However,

microscale strain effects for the Re_L = 1000 case appeared to be significant in reducing the instantaneous flame temperature. Consequently, the reduction in peak values seen in Figures 9 – 12 are a result of nonequilibrium effects introduced by microscale strain, and by the broadening of the mixture fraction pdfs for these cases. This broadening effect on the mixture fraction pdfs is characteristic of the increase in mixture fraction fluctuations seen in Figure 13. This is an interesting result from the perspective that this modeling formulation can distinguish between a reduction in mean temperature and product formation due to microscale strain (i.e., Re_L) and nonequilibrium effects resulting from large scale flame straining (i.e., <*a*>). This point again illustrates the unique capability of this modeling formulation.

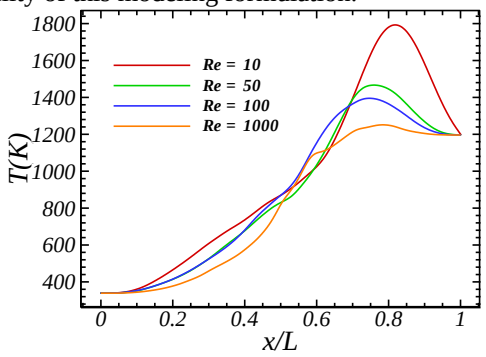

Figure 9. Mean temperature variation with Re_L plotted as a function of *x/L* at <*a*> = 1056 1/sec.

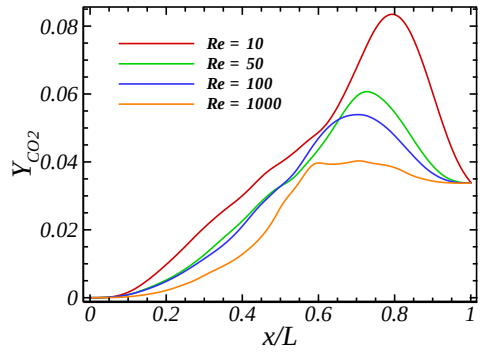

Figure 10. Mean CO_2 mass fraction variation with Re_L plotted as a function of *x/L* at <*a*> = 1056 1/sec.

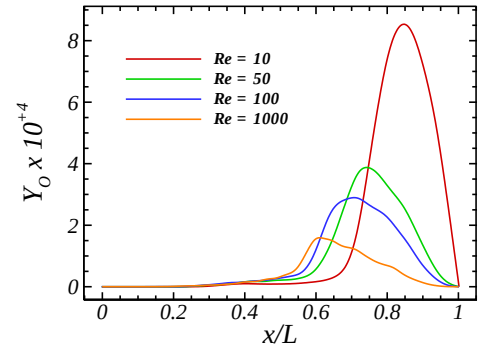

Figure 11. Mean O mass fraction variation with Re_L plotted as a function of *x/L* at <*a*> = 1056 1/sec.

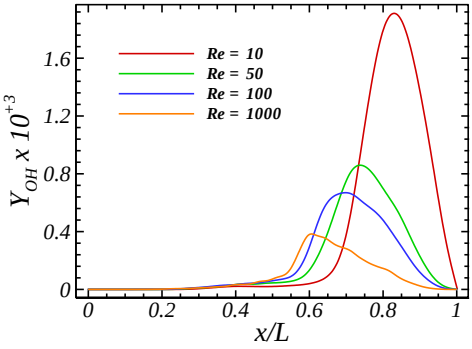

Figure 12. Mean OH mass fraction variation with Re_L plotted as a function of *x/L* at <*a*> = 1056 1/sec.

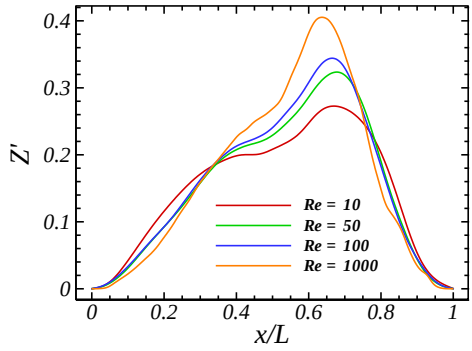

Figure 13. Mixture fraction fluctuations as a function of *x/L* at <*a*> = 1056 1/sec.

With the LEM statistical data generated for the simulation matrix given in Table A1, a parameterized LEM model database may be constructed. There are two approaches to generating such a model database. These are *reduced* and *full* parameterization. Within the reduced parameterization approach, the model provides statistics for the filtered species and possibly a filtered reaction progress variable. These statistics are parameterized in terms of a relatively small number of variables such as the filtered mixture fraction (<ξ>), scalar dissipation (<χ>), and subgrid scale Reynolds number (Re_Δ). This type of parameterization is very similar to flamelet modeling [2], except for the fact that within the LEM approach the underlying scalar pdf is *predicted* and not *assumed*. The *full* parameterization approach, however, directly models *all* the filtered reaction rates within the chemical mechanism. This approach will naturally entail a large number of parameters to accurately characterize the statistics. The full parameterization approach is more general, but is limited by the number of species transport equations that may be tractably solved during a LES. As a result, the full parameterization approach may not be applied to large chemical mechanisms due to the computational cost involved with the solution of a large number of species transport equations. The reduced parameterization approach, however, may be applied to arbitrarily large chemical mechanisms because the flow solver is only required to solve a limited set of transport equations. The LEM-CF modeling formulation may be applied to either the reduced or full parameterization approaches.

To illustrate the development of a parameterized LEM combustion model from the LEM-CF data, a reduced

parameterization approach was chosen. The strategy used to construct a database for the subgrid model followed that of Sankaran, et al. [11], who parameterized the mean species in terms of mean mixture fraction, mean scalar dissipation, and Reynolds number. As mentioned earlier, LEM data from that study were generated for homogeneous turbulence in the absence of mean strain. With the LEM-CF formulation, however, mean strain effects may be directly included within the parameterization. Consequently, the parameterization approach of Sankaran, et al. [11] was modified by replacing the scalar dissipation with the strain rate as,

$$< Y_k >= f(< Z >, < a >, Re_L) \quad (14)$$

With this form of parameterization, strain rate effects that lead to local extinction are directly included within the formulation.

As discussed by Sankaran, et al. [11], application of these types of parameterization strategies to LES modeling is straight forward. The mean mixture fraction, mixture fraction variance, mean scalar dissipation and mean strain rate from the LEM are directly related to the LES filtered values of these quantities. As noted by Sankaran, et al. [11], since the mean quantities are computed directly from the LEM predicted scalar pdf, there is no need for any a posteriori model to link the instantaneous scalar distributions with the mean values, as is required for the flamelet model [2]. The LES subgrid Reynolds number (Re_Δ) is also directly related to the LEM Reynolds number as $Re_\Delta = Re_L$, with Re_Δ being defined as,

$$Re_\Delta = \frac{u'\Delta}{(\nu_{FUEL} + \nu_{OXI})/2} \quad (15)$$

where u' is specified in terms of the subgrid turbulent kinetic energy (k_{sgs}) as $u' = \sqrt{2k_{sgs}/3}$. With this form of the Reynolds number, the LES and LEM-CF values are consistent and unambiguously defined in terms of the reference values (ν_{FUEL}, ν_{OXI}) of the viscosity. The LEM-CF strain rate ($<a>$) is specified from the LES as $<a>=<a>_{LES}$, where $<a>_{LES}$ is the magnitude of the local resolved scale strain rate (S_{ij}) with $< a >_{LES} = \sqrt{S_{ij}S_{ij}}$.

The parameterization strategy defined by Eqn. (14) offers an additional benefit beyond that of the strategy proposed by Sankaran, et al. [11] regarding LES modeling of the input parameters. The mean or filtered scalar dissipation, $<\chi>$ must be supplied from the LES code using an addition model for this quantity. The mean or resolved scale strain rate, $<a>$, in Eqn. (14), however, may be directly calculated from the LES resolved scale velocity field. This removes the model uncertainty associated with the specification of $<\chi>$.

Given the parameterization defined by Eqn. (14), the LEM data generated from the results of the simulation matrix detailed in Table A1 were organized as a function of these three parameters. For example, Figures 14 and 15 present CO_2 and OH mass fraction as a function of mixture fraction and Reynolds number at a mean strain rate of $<a>$ = 1056 1/sec, respectively. These figures represent a re-plot of the data in Figures 10 and 12, respectively, but with the laminar flow results included. As may be seen from these figures, the primary effect of the turbulence is to broaden the flame structure in mixture fraction space and reduce the maximum realized scalar values, as discussed earlier. Figure 16 and 17 present these species plotted as a function of mixture fraction at different strains rates for Re_L = 50. These figures are a re-plot of the data in Figures 5 and 7 as a function of mixture fraction. The post extinction values at $<a>$ = 5095 1/sec are clearly evident in these figures.

With the LEM simulation data processed as shown, for example, in Figures 14 – 17, a model database may then be created that conforms to the parameterization strategy defined by Eqn. (14). The model data were stored in a *binary space partition* (BSP) [20] binary tree. This type of database structure was used by Pope [21] for the *in situ adaptive tabularization* (ISAT) approach to chemical kinetic source term time integration. Each data point within a BSP tree has a set of inputs or "keys," and an associated set of output data. Given the data in this form, a series of cutting planes are defined that segregate the data with respect to the input keys. These cutting planes define the "branches" of the binary tree structure which eventually lead to "leaves" or data nodes. The methodology used to construct a BSP database is described in detail by Pope [21] and is not repeated here for brevity. A BSP tree is used to construct a database of the LEM statistical data based on the input keys of $<Z>$, $<a>$ and Re_L. Output data for each entry in the tree are the mean species $<Y_k>$ that are required by the flow solver, as well as post processing data such as the species fluctuations.

The BSP tree structure used for the LEM data in this study follows that of Pope [21], except for one modification. The BSP tree employed here included multiple data points on each data node or leaf. Each data node contained eight data points, which from prior experience with ISAT implementations [20] provides for efficient tree searching and data retrieval. Given a set of input query keys, the outputs are generated by searching the BSP tree using the cutting planes to find the appropriate leaf or data node. Once the data node is identified, a distance weighted interpolation algorithm is then used to create the outputs given all the data points on that node. The extinction limits defined in Table A1 are implemented by adding additional entries into the database for each Reynolds number that correspond to the nonreacting or extinguished solution at the global extinction limit. These additional entries include an arbitrarily large value of strain rate that is beyond that of the extinction limit. By adding this additional data to the BSP tree database, any query point with a strain rate higher than the extinction limit will find a data node that is nonreacting from which to create the outputs using the distance weighted interpolation. The BSP tree database then constitutes a completed LEM parameterized model that may be deployed within a CFD flow solver.

The final BSP database generated from the data was approximately 13 Mbytes in size. The database for this case is relatively small and could be directly deployed within a LES solver. However, the database size will rapidly grow as more detailed or expanded parameterization strategies are employed. Large databases may be modeled using a collection of artificial neural networks. Artificial neural network (ANN) methodology is a data modeling technique specialized for high

dimensional, highly nonlinear data sets. Sen and Menon [12] used a collection of ANNs to model a LEM database that included ~ 24 input parameters. Using that approach, a large reduction in memory requirements may be achieved while maintaining an efficient and accurate data retrieval methodology.

The enhanced physics captured by the LEM-CF formulation compared to the flamelet model comes at a significant computational cost. The computational cost of a LEM-CF case was roughly fifty times more expensive than a corresponding flamelet simulation for the same conditions. This additional cost is primarily a result of the time required to converge the LEM statistics. Also, the computational cost increases with Re_L due to the requirement that the Kolmogorov microscale be resolved. From Table A1, the Re_L = 1000 cases used approximately three times the number of points as the lower Re_L cases. Even with the additional cost of the LEM-CF formulation, all the simulations listed in Table A1 could be completed overnight on a modern Linux cluster.

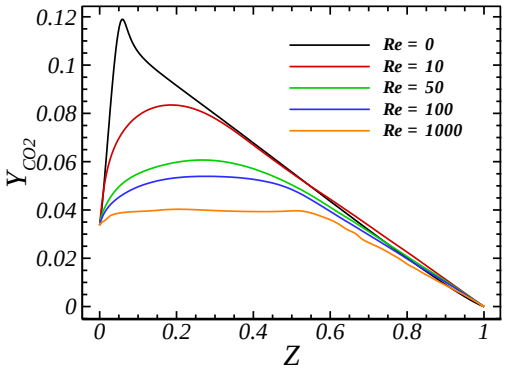

Figure 14. Mean CO_2 mass fraction variation as a function of mixture fraction and Reynolds number at <*a*> = 1056 1/sec.

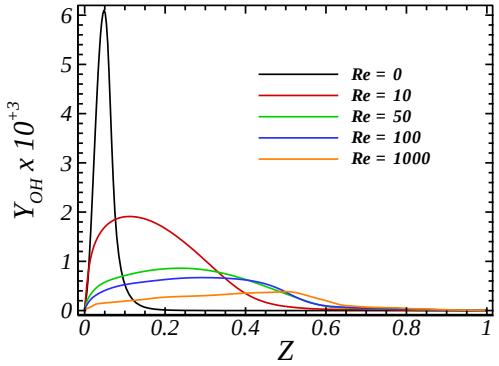

Figure 15. Mean OH mass fraction variation as a function of mixture fraction and Reynolds number at <*a*> = 1056 1/sec.

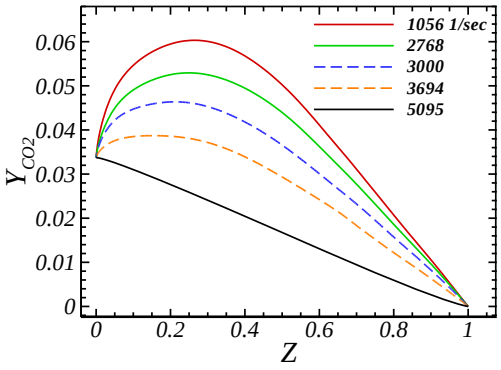

Figure 16. Mean CO_2 mass fraction as a function of mixture fraction and mean strain rate at Re_L = 50.

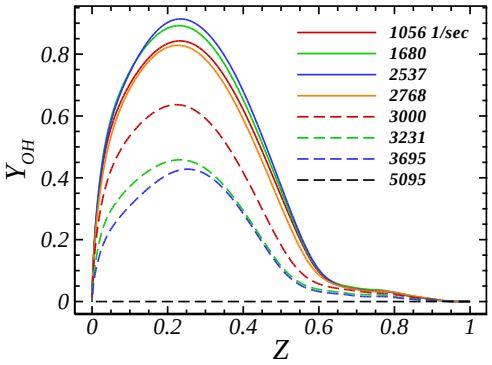

Figure 17. Mean OH mass fraction as a function of mixture fraction and mean strain rate at Re_L = 50.

CONCLUSIONS AND RECOMMENDATIONS

This effort has addressed the development of a unique sub-modeling formulation that may be used to generate parameterized subgrid combustion models for LES. This sub-model formulation is based on a novel application of the LEM turbulent combustion model to the counter flow configuration. This formulation may then be used to generate the required statistics to create an efficient subgrid model for LES. The principle conclusions from this study are summarized below.

1. A unique application of the LEM turbulent combustion model to the counter flow configuration may be applied to the prediction of turbulent flame extinction limits that result from both small and large scale turbulent strain effects.
2. The new LEM/counter flow (LEM-CF) formulation is unique from the perspective that no other methodology exist to predicts turbulent flame extinction due to resolved scale strain except a full 3-D direct numerical simulation (DNS). However, application of DNS to Reynolds that may be simulated with the LEM-CF model is intractable due to grid resolution requirements.
3. Using the LEM-CF formulation, LES closure statistics may be generated that directly include the effects of subgrid Reynolds number and resolved scale strain rate.

This includes a prediction of the turbulent flame extinction limits.

4. The LEM-CF methodology was successfully applied to generate a parameterized LEM combustion model for augmentor conditions, thereby demonstrating the feasibility of this approach.

The follow recommendations are made to fully develop this approach as an LES subgrid model:

1. The new LEM-CF sub-model formulation should be applied to turbulent counter flow jet experiments to validate the formulation and provide confidence in the accuracy of the methodology.
2. ANN data modeling methodology should be applied to model the LEM-CF databases to reduce the anticipated computer memory requirements of this formulation.
3. The new subgrid model formulation needs to be validated for a series of test cases that include fully attached flames, flames near extinction, and to predict blow-out limits.

ACKNOWLEDGEMENTS

The authors gratefully acknowledge Dr. Balu Sekar and Dr. Barry Kiel of AFRL/RZTC, Wright-Patterson Air Force Base for supporting this research under an AFRL Phase I SBIR program.

REFERENCES

[1] Byggstøyl, S. and Magnussen, B.F., "A Model for Flame Extinction in Turbulent Flow," in *Turbulent Shear Flows 4*, eds. Bradury et al., Springer-Verlag, New York, pp. 381–395, 1983.

[2] Peters, N., *Turbulent Combustion*, Cambridge University Press, Cambridge, UK, 2000.

[3] Menon, S. and Calhoon, W.H. Jr., "Subgrid Mixing and Molecular Transport Modeling in a Reacting Shear Layer," *Twenty-Sixth Symposium (International) on Combustion*, The Combustion Institute, pp. 59 - 66, 1996.

[4] Chakravarthy, V. K. and Menon, S., "Linear-Eddy Simulations of Reynolds and Schmidt Number Dependencies in Turbulent Scalar Mixing," *Physics of Fluids*, Vol. 13, pp. 488–499, 2001.

[5] Jaberi, F.A., Colucci, P.J., James, S., Givi, P., Pope, S.B., "Filtered mass density function for large-eddy simulation of turbulent reacting flows," *Journal of Fluid Mechanics*, Vol. 401, 1999, pp. 85 – 121.

[6] Kerstein, A. R., "Linear-Eddy Model of Turbulent Transport II. Application to Shear Layer Mixing," *Combustion and Flame*, Vol. 75, pp. 397–413, 1989.

[7] Kerstein, A. R., "Linear-Eddy Model of Turbulent Transport 4. Structure of Diffusion-Flames," *Combustion Science and Technology*, Vol. 81, pp. 75–96, 1992.

[8] Goldin, G.M. and Menon, S., "A Scalar PDF Construction Model for Turbulent Non-Premixed Combustion," *Combustion Science and Technology*, Vol. 125, pp. 47–72, 1997.

[9] Goldin, G.M. and Menon, S., "A Comparison of Scalar PDF Turbulent Combustion Models," *Combustion and Flame*, Vol. 113, pp. 442–453, 1998.

[10] Goldin, G.M. and Raman, V., "A Constructed PDF Model for Fast CFD with Realistic Chemistry," *Proceedings of the Summer Program 2004*, Center for Turbulence Research, Stanford University, Stanford, CA, 2004.

[11] Sankaran, V., Drozda, T.G., and Oefelein, J.C., "A Tabulated Closure for Turbulent Non-premixed Combustion Based on the Linear Eddy Model," *Proceeding of the Combustion Institute*, Vol. 32, 2009, pp. 1571 – 1578.

[12] Sen, B.A. and Menon, S., "Artificial Neural Networks Based Chemistry-Mixing Subgrid Model for LES", 47th AIAA Aerospace Sciences Meeting, Jan. 5 – 8, 2009, Orlando, FL.

[13] Calhoon, W.H. Jr, "On Subgrid Combustion Modeling for Large-Eddy Simulations," *Ph.D. Thesis*, Georgia Institute of Technology, Atlanta, GA, 1996.

[14] Im, H. G., Raja, L. L., Kee, R. J., Lutz, A. E., Petzold, L. R., "OPUS: A Fortran Program for Unsteady Opposed-Flowed Flames," *Sandia Report SAND2000-8211*, Sandia National Laboratories, July, 2000.

[15] Pope, S. B, *Turbulent Flows*, Cambridge University Press, Cambridge, UK, 2000.

[16] Kee, R. J., Dixon-Lewis, G., Warnatz, J., Coltrin, M.E., and Miller, J. A., "A Fortran Computer Code Package for the Evaluation of Gas-Phase Multicomponent Transport Properties," *Sandia Report SAND86-8246*, Sandia National Laboratories, Sept., 1991.

[17] Smooke, M. D., Puri, I. K., and Seshadri, K. "A Comparison Between Numerical Calculations and Experimental Measurements of the Structure of a Counterflow Diffusion Flame Burning in Diluted Air," *Twenty-first Symposium (International) on Combustion*, The Combustion Institute, pp. 1783–1792, 1986.

[18] Schlichting, H., *Boundary-Layer Theory*, McGraw-Hill Book Company, New York, 1979.

[19] Zambon, A.C. and Chelliah, H.K., "Explicit reduced reaction models for ignition, flame propagation, and extinction of $C_2H_4/CH_4/H_2$ and air systems", *Combustion and Flame*, 150 (2007), pp. 71 – 91.

[20] Calhoon, W.H. and Zambon, A.C., "Efficiency Enhancements for Chemical Kinetics in Rocket Plumes," proceeding of the JANNAF 30th Exhaust Plume Technology Subcommittee Meeting, Newton, MA, May 12 – 16, 2008.

[21] Pope, S. B., "Computationally Efficient Implementation of Combustion Chemistry Using In Situ Adaptive Tabularization," *Combustion Theory and Modeling*, Vol. 1, 1997, pp. 41–63.

[22] Zhao, R. and Smits, A. J., "Scaling of the wall-normal turbulent component in high-Reynolds-number pipe flow," *Journal of Fluid Mechanics*, Vol. 576, 2007, pp. 457 – 473.

Appendix I

As discussed earlier, several assumptions are needed to relate the LEM for the counter flow configuration to an actual counter flow experiment, and to the LES subgrid. These assumptions again are:

1) L is equal to the jet separation distance, X_L.
2) For turbulent counter flow conditions, the jets exhaust from fully developed turbulent pipe flows.
3) L is also equal to the centerline mixing length, l_T, for fully developed turbulent pipe flow.
4) u' is equal to the centerline axial velocity fluctuation for fully developed turbulent pipe flow.
5) The jet momenta are assumed equal.

With the first assumption, L is related to the jet separation width X_L as,

$$L = X_L \tag{A1}$$

With the second and third assumptions, the centerline turbulent mixing length in pipe flows is given empirically by, [18]

$$\frac{l_T}{D} \sim 0.07 \tag{A2}$$

which is independent of Reynolds number [18]. The turbulent length scale, L, is then given by,

$$L = l_T \sim (0.07)D \tag{A3}$$

Eqns. (A1) and (A3) now establish a relationship between the jet diameter, separation distance, and the LEM integral length scale.

With the fourth assumption, the velocity fluctuation (u') may be determined from experimental correlations. From Zhao and Smits [22], the centerline axial velocity fluctuation in fully developed pipe flow scales as,

$$\frac{u'}{u_\tau} = M_0 \sim 0.816 \tag{A4}$$

and is independent of Reynolds number. The friction velocity, u_τ, in Eqn. (A4) is defined by,

$$u_\tau = \sqrt{\frac{\tau_w}{\rho}} \tag{A5}$$

where τ_w is the wall shear stress. From Schlichting [18], τ_w for fully developed pipe flow is empirically given by,

$$\tau_w = C_0 \rho u_B^{7/4} \nu^{1/4} D^{-1/4},\ C_0 = 0.03955 \tag{A6}$$

where u_B is the pipe bulk velocity. With Eqns. (A4) – (A6), the following relationship for u' may be derived,

$$u' = M_0^{1/2} C_0^{1/2} (u_B^{7/8} \nu^{1/8}) D^{-1/8} \tag{A7}$$

The term $(u_B^{7/8}\nu^{1/8})$ in this equation is taken as the maximum value from the two jet streams because the maximum u' will determine the fluctuation level within the counter flow jet domain.

With Eqns. (10), (A1), (A3) and (A7), a relationship for the jet nozzle exit diameter in terms of the LEM Reynolds number and jet velocity may be derived yielding,

$$D = \left[\frac{Re_L (\nu_{FUEL} + \nu_{OXI})/2}{(0.07) M_0^{1/2} C_0^{1/2} (u_B^{7/8} \nu^{1/8})} \right]^{8/7} \tag{A8}$$

With the diameter determined, the jet separation distance and LEM length scale are found from Eqns. (A1) and (A3). The jet nozzle Reynolds numbers are then given by,

$$Re_{fuel} = \frac{u_{FUEL} D}{\nu_{FUEL}},\ Re_{OXI} = \frac{u_{OXI} D}{\nu_{OXI}} \tag{A9}$$

The fifth assumption results in the following relationship,

$$\rho_{FUEL} \left(u_{FUEL}\right)^2 = \rho_{OXI} \left(u_{OXI}\right)^2 \tag{A10}$$

Eqns. (11), (A1), (A3), (A8) and (A10) may be combined into a system of nonlinear equations that may be solved to obtain u_{FUEL}, u_{OXI}, X_L, L and D given the jet thermodynamics conditions and Re_L and <a>.

Appendix II

Table A1: LEM-CF Simulation Matrix for Augmentor Conditions

Case no.	Re_L	<a> (1/sec)	L (cm)	u_{FUEL} (cm/sec)	u_{OXI} (cm/sec)	D (cm)	Re_{FUEL}	Re_{OXI}	*Ext.*
1	0.	1.0563E+03	1.0000E+00	3.7032E+02	6.8603E+02	n/a	n/a	n/a	No
2	0.	1.6800E+03	1.0000E+00	5.8898E+02	1.0911E+03	n/a	n/a	n/a	No
3	0.	2.5369E+03	1.0000E+00	8.8938E+02	1.6475E+03	n/a	n/a	n/a	No
4	0.	3.6945E+03	1.0000E+00	1.2951E+03	2.3993E+03	n/a	n/a	n/a	No
5	0.	5.0946E+03	1.0000E+00	1.7860E+03	3.3086E+03	n/a	n/a	n/a	No
6	0.	6.6681E+03	1.0000E+00	2.3376E+03	4.3305E+03	n/a	n/a	n/a	No
7	0.	8.4966E+03	1.0000E+00	2.9786E+03	5.5179E+03	n/a	n/a	n/a	No
8	0.	1.0363E+04	1.0000E+00	3.6329E+03	6.7300E+03	n/a	n/a	n/a	No
9	0.	1.7010E+04	1.0000E+00	5.9632E+03	1.1046E+04	n/a	n/a	n/a	Yes
10	0.	1.7500E+04	1.0000E+00	6.1349E+03	1.1365E+04	n/a	n/a	n/a	Yes
11	10.	1.0563E+03	2.0698E-01	7.6651E+01	1.4199E+02	2.9569E+00	7.8749E+03	1.0094E+03	No
12	10.	1.6800E+03	1.6412E-01	9.6668E+01	1.7907E+02	2.3446E+00	7.8749E+03	1.0094E+03	No
13	10.	2.5369E+03	1.3356E-01	1.1878E+02	2.2005E+02	1.9080E+00	7.8749E+03	1.0094E+03	No
14	10.	2.7685E+03	1.2785E-01	1.2409E+02	2.2987E+02	1.8265E+00	7.8749E+03	1.0094E+03	No
15	10.	3.0000E+03	1.2282E-01	1.2917E+02	2.3929E+02	1.7546E+00	7.8749E+03	1.0094E+03	No
16	10.	3.2315E+03	1.1834E-01	1.3406E+02	2.4835E+02	1.6906E+00	7.8749E+03	1.0094E+03	No
17	10.	3.4630E+03	1.1431E-01	1.3878E+02	2.5710E+02	1.6331E+00	7.8749E+03	1.0094E+03	No
18	10.	3.6945E+03	1.1067E-01	1.4334E+02	2.6555E+02	1.5811E+00	7.8749E+03	1.0094E+03	No
19	10.	5.0946E+03	9.4250E-02	1.6833E+02	3.1184E+02	1.3464E+00	7.8749E+03	1.0094E+03	No
20	10.	6.6681E+03	8.2383E-02	1.9258E+02	3.5676E+02	1.1769E+00	7.8749E+03	1.0094E+03	Yes
21	50.	1.0563E+03	5.1921E-01	1.9228E+02	3.5620E+02	7.4173E+00	4.9552E+04	6.3520E+03	No
22	50.	1.6800E+03	4.1170E-01	2.4249E+02	4.4921E+02	5.8815E+00	4.9552E+04	6.3520E+03	No
23	50.	2.5369E+03	3.3503E-01	2.9797E+02	5.5200E+02	4.7862E+00	4.9552E+04	6.3520E+03	No
24	50.	2.7685E+03	3.2072E-01	3.1127E+02	5.7664E+02	4.5817E+00	4.9552E+04	6.3520E+03	No
25	50.	3.0000E+03	3.0810E-01	3.2403E+02	6.0027E+02	4.4014E+00	4.9552E+04	6.3520E+03	No
26	50.	3.2315E+03	2.9685E-01	3.3630E+02	6.2300E+02	4.2408E+00	4.9552E+04	6.3520E+03	No
27	50.	3.4630E+03	2.8676E-01	3.4814E+02	6.4493E+02	4.0966E+00	4.9552E+04	6.3520E+03	No
28	50.	3.6945E+03	2.7763E-01	3.5959E+02	6.6614E+02	3.9662E+00	4.9552E+04	6.3520E+03	No
29	50.	3.8103E+03	2.7338E-01	3.6518E+02	6.7650E+02	3.9054E+00	4.9552E+04	6.3520E+03	No
30	50.	3.9260E+03	2.6932E-01	3.7068E+02	6.8669E+02	3.8474E+00	4.9552E+04	6.3520E+03	No
31	50.	4.0418E+03	2.6543E-01	3.7611E+02	6.9674E+02	3.7919E+00	4.9552E+04	6.3520E+03	No
32	50.	5.0946E+03	2.3642E-01	4.2226E+02	7.8225E+02	3.3775E+00	4.9552E+04	6.3520E+03	Yes
33	50.	6.6681E+03	2.0665E-01	4.8309E+02	8.9493E+02	2.9522E+00	4.9552E+04	6.3520E+03	Yes
34	100.	1.0563E+03	7.7155E-01	2.8572E+02	5.2931E+02	1.1022E+01	1.0942E+05	1.4026E+04	No
35	100.	1.6800E+03	6.1179E-01	3.6033E+02	6.6753E+02	8.7399E+00	1.0942E+05	1.4026E+04	No
36	100.	2.5369E+03	4.9786E-01	4.4279E+02	8.2028E+02	7.1123E+00	1.0942E+05	1.4026E+04	No
37	100.	2.7685E+03	4.7659E-01	4.6255E+02	8.5689E+02	6.8084E+00	1.0942E+05	1.4026E+04	No
38	100.	3.0000E+03	4.5783E-01	4.8151E+02	8.9200E+02	6.5405E+00	1.0942E+05	1.4026E+04	No
39	100.	3.2315E+03	4.4113E-01	4.9974E+02	9.2578E+02	6.3018E+00	1.0942E+05	1.4026E+04	No
40	100.	3.4630E+03	4.2613E-01	5.1733E+02	9.5837E+02	6.0875E+00	1.0942E+05	1.4026E+04	No
41	100.	3.6945E+03	4.1256E-01	5.3435E+02	9.8988E+02	5.8937E+00	1.0942E+05	1.4026E+04	Yes
42	100.	5.0946E+03	3.5132E-01	6.2748E+02	1.1624E+03	5.0189E+00	1.0942E+05	1.4026E+04	Yes
43	100.	6.6681E+03	3.0709E-01	7.1787E+02	1.3298E+03	4.3870E+00	1.0942E+05	1.4026E+04	Yes
44	1000.	1.0563E+03	2.8760E+00	1.0650E+03	1.9730E+03	4.1086E+01	1.5204E+06	1.9489E+05	No
45	1000.	1.6800E+03	2.2805E+00	1.3431E+03	2.4882E+03	3.2578E+01	1.5204E+06	1.9489E+05	No
46	1000.	1.9656E+03	2.1083E+00	1.4528E+03	2.6914E+03	3.0119E+01	1.5204E+06	1.9489E+05	No
47	1000.	2.2513E+03	1.9700E+00	1.5548E+03	2.8803E+03	2.8143E+01	1.5204E+06	1.9489E+05	No
48	1000.	2.5369E+03	1.8558E+00	1.6505E+03	3.0576E+03	2.6512E+01	1.5204E+06	1.9489E+05	Yes
49	1000.	2.6141E+03	1.8282E+00	1.6754E+03	3.1038E+03	2.6117E+01	1.5204E+06	1.9489E+05	Yes
50	1000.	2.7685E+03	1.7765E+00	1.7242E+03	3.1941E+03	2.5379E+01	1.5204E+06	1.9489E+05	Yes